PHYSICAL REVIEW B **93**, 180510(R) (2016)

Coupled motion of Xe clusters and quantum vortices in He nanodroplets

Curtis F. Jones,[1] Charles Bernando,[2] Rico Mayro P. Tanyag,[1] Camila Bacellar,[3,4] Ken R. Ferguson,[5,6] Luis F. Gomez,[1,*] Denis Anielski,[7,8] Ali Belkacem,[3] Rebecca Boll,[7,8,9] John Bozek,[5] Sebastian Carron,[5] James Cryan,[3] Lars Englert,[10] Sascha W. Epp,[11] Benjamin Erk,[7,8,9] Lutz Foucar,[7,12] Robert Hartmann,[13] Daniel M. Neumark,[3,4] Daniel Rolles,[7,9,12,†] Artem Rudenko,[7,8,†] Katrin R. Siefermann,[3,‡] Fabian Weise,[3,§] Benedikt Rudek,[7,8,14] Felix P. Sturm,[3] Joachim Ullrich,[7,8,14] Christoph Bostedt,[5,15,16,17,‖] Oliver Gessner,[3,¶] and Andrey F. Vilesov[1,2,**]

[1]*Department of Chemistry, University of Southern California, Los Angeles, California 90089, USA*
[2]*Department of Physics and Astronomy, University of Southern California, Los Angeles, California 90089, USA*
[3]*Chemical Sciences Division, Lawrence Berkeley National Laboratory, Berkeley, California 94720, USA*
[4]*Department of Chemistry, University of California Berkeley, Berkeley, California 94720, USA*
[5]*Linac Coherent Light Source, LCLS, SLAC National Accelerator Laboratory, 2575 Sand Hill Road, Menlo Park, California 94025, USA*
[6]*Department of Applied Physics, Stanford University, Stanford, California 94063, USA*
[7]*Max Planck Advanced Study Group at the Center for Free-Electron Laser Science (CFEL), Notkestraße 85, 22607 Hamburg, Germany*
[8]*MaxPlanck-Institut für Kernphysik, Saupfercheckweg 1, 69117 Heidelberg, Germany*
[9]*Deutsches Elektronen-Synchrotron (DESY), Notkestraße 85, 22607 Hamburg, Germany*
[10]*Max-Planck-Institut für extraterrestrische Physik, Giessenbachstraße, 85741 Garching, Germany*
[11]*Max-Planck-Institut für Struktur und Dynamik der Materie, Luruper Chaussee 149, 22761 Hamburg, Germany*
[12]*Max-Planck-Institut für Medizinische Forschung, Jahnstrasse 29, 69120 Heidelberg, Germany*
[13]*PNSensor GmbH, Otto-Hahn-Ring 6, 81739 München, Germany*
[14]*Physikalisch-Technische Bundesanstalt, Bundesallee 100, D-38116 Braunschweig, Germany*
[15]*PULSE Institute, Stanford University and SLAC National Accelerator Laboratory, 2575 Sand Hill Road, Menlo Park, California 94025, USA*
[16]*Argonne National Laboratory, 9700 South Cass Avenue B109, Lemont, Illinois 60439, USA*
[17]*Department of Physics and Astronomy, Northwestern University, 2145 Sheridan Road, Evanston, IL 60208, USA*

(Received 19 May 2015; revised manuscript received 2 May 2016; published 26 May 2016)

Single He nanodroplets doped with Xe atoms are studied via ultrafast coherent x-ray diffraction imaging. The diffraction images show that rotating He nanodroplets about 200 nm in diameter contain a small number of symmetrically arranged quantum vortices decorated with Xe clusters. Unexpected large distances of the vortices from the droplet center (≈0.7–0.8 droplet radii) are explained by a significant contribution of the Xe dopants to the total angular momentum of the droplets and a stabilization of widely spaced vortex configurations by the trapped Xe clusters.

DOI: 10.1103/PhysRevB.93.180510

Quantum vortices are the hallmark of superfluidity [1–3]; they represent fundamental excitations of a superfluid and often define its physical properties. Quantum vortices form a lattice in a rotating container filled with superfluid helium, and they are responsible for turbulent superfluid flow in various experiments [2–4]. More recently, studies of superfluidity have been extended towards nanoscale systems [5,6]. The observation of sharp rotational lines for molecules encapsulated in He nanodroplets with radii $\leqslant 5$ nm provided the first evidence for the superfluid nature of such droplets [5,7]. However, these experiments were insensitive to the rotational excitation of the host droplets. *Ex situ* transmission electron microscopy studies of metallic dopant residues deposited on a carbon foil by droplet impact uncovered the formation of metal nanowires in 1-μm-sized ^{4}He droplets, a phenomenon ascribed to aggregation of metal clusters along the cores of quantum vortices [6,8,9]. Very recently, ultrafast single-shot x-ray diffraction imaging of Xe doped He droplets employing an x-ray free electron laser (XFEL) revealed Bragg spots, confirming the existence of quantum vortex lattices that enabled the condensation of 100–200 Xe clusters in a periodic array [10]. While these findings provide evidence that quantum vortices exist in droplets as small as a few microns in diameter, Bragg spots provide only information about the global cluster/vortex arrangement in large droplets and obscure the details of individual vortex placements.

In an effort to study the regime of quantum rotation in smaller, self-contained, superfluid systems, we expand the previous x-ray coherent diffraction imaging studies [10] to droplets with ≈100 nm radii. The positions of vortices were deduced from diffraction images lacking Bragg spots using the recently developed phase retrieval algorithm for coherent diffraction imaging in droplets (DCDI) [11]. We report the determination of vortex configurations inside such droplets doped with Xe atoms and demonstrate that the presence of a few vortices induces the formation of multiple Xe clusters that occupy symmetric positions far away from the droplet centers.

*Present address: IPG Photonics, 3930 Freedom Circle, Ste. 130, Santa Clara, California 95054, USA.
†Present address: J. R. MacDonald Laboratory, Department of Physics, Kansas State University, Manhattan, Kansas 66506, USA.
‡Present address: Leibniz Institute of Surface Modification (IOM), Permoserstraße 15, 04318 Leipzig, Germany.
§Present address: Berliner Glas KGaA Herbert Kubatz GmbH & Co., Waldkraiburger Str. 5, 12347 Berlin, Germany.
‖cbostedt@anl.gov.
¶ogessner@lbl.gov
**vilesov@usc.edu

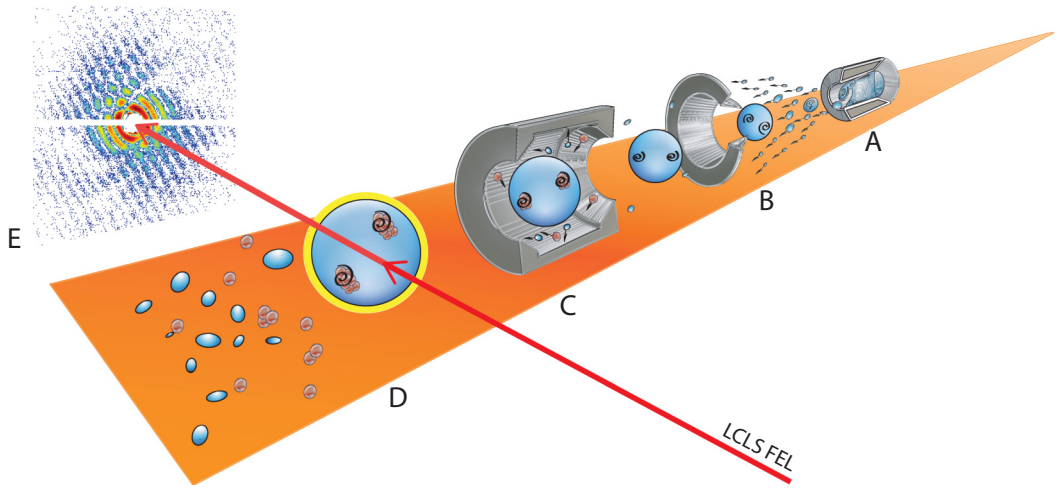

FIG. 1. Experimental layout. (A) Rotating droplets are formed upon expansion of liquid He into vacuum; (B) quantum vortices are formed upon evaporative cooling of the droplets to below T_λ; (C) droplets are doped with Xe atoms when passing through a cell filled with Xe gas; (D) a single doped droplet is irradiated by a single x-ray pulse from an XFEL; and (E) the x-ray diffraction pattern is recorded by a pnCCD detector.

The vortex configurations give access to the rotational energy, angular momentum, and angular velocity of the nanodroplets, as well as the coupling between the rotational motion of the host droplet and the dopant Xe clusters, the details of which remain largely undiscovered.

Figure 1 shows the experimental layout [10]. The method of helium nanodroplet formation and subsequent doping has been extensively documented elsewhere [6,12–14]. In brief, a continuous beam of superfluid He nanodroplets was generated by expanding liquid ^{4}He at temperatures $T < 7$ K and a backing pressure of 20 bars through a 5 μm orifice into high vacuum. The fluid exiting the nozzle fragmented into droplets that cooled via evaporation to 0.38 K [7], reaching final average sizes of $N_{\mathrm{He}} \approx 10^8$ He atoms (radii $R_D \approx 100$ nm). Each droplet was doped with $N_{\mathrm{Xe}} \approx 10^5$ Xe atoms upon passing through room temperature Xe gas inside a pick-up cell. The determination of N_{Xe} is described in the Supplemental Material (SM) [15]. Following capture by the droplet, Xe atoms cluster along the vortex cores [8–10,16] and act as a contrast agent. Further downstream, the droplet beam crossed the XFEL beam near the focus (≈5 μm diameter) of the AMO beamline at the Linac Coherent Light Source (LCLS) [17,18]. X-ray pulses of 100 fs duration, each containing ≈10^{12} 1.5 keV photons ($\lambda = 0.826$ nm), were diffracted from single, doped droplets resulting in characteristic patterns that were imaged by the high-resolution pnCCD x-ray camera of the CAMP instrument [19]. The image plane was located 565 mm behind the interaction point on the XFEL beam axis.

Figure 2(A1) shows the diffraction image from an undoped He droplet with a radius of 115 nm that has a circular projection in the detector plane. The image consists of a series of concentric circular rings. Images from droplets doped with Xe atoms are shown in Figs. 2(B1)–2(F1). They contain high contrast diffraction patterns that emerge from the interference of scattering signals from He droplets and their Xe content. Figures 2(B1)–2(D1), in particular, exhibit striking symmetries that invite rationalization in terms of corresponding symmetric Xe cluster configurations, which may be estimated by modeling [20] as described in the SM [15]. In general, however, the DCDI iterative phase retrieval algorithm [11] is applied in order to obtain the density distributions of the Xe clusters from the diffraction images. Briefly, DCDI represents a modified error reduction algorithm [21] that iteratively performs Fourier and inverse Fourier transforms while optimizing the agreement between a simulated and the measured diffraction patterns within boundary conditions set by several physical constraints. DCDI takes advantage of the fact that the scattering signals in Figs. 2(B1)–2(F1) contain considerable contributions from the droplet itself, which enables an approximate phasing and serves as a good starting point for the iterative phase retrieval. The results are projections of the Xe densities onto the detector plane [10] as shown in Figs. 2(A2)–2(F2). The black contours represent the droplets' boundaries. The density images consist of 6.4 × 6.4 nm^2 pixels that are defined by the number and size of the CCD pixels, the distance of the CCD from the scattering center, and the wavelength of the x rays. The resolution of the images corresponds to approximately 3 pixels or ≈20 nm. The calculated diffraction patterns in Figs. 2(A3)–2(F3) are retrieved from the density distributions in Figs. 2(A2)–2(F2). Their excellent agreement with the measured patterns in Figs. 2(A1)–2(F1) demonstrates the self-consistency of the reconstruction procedure.

All diffraction patterns in Figs. 2(A1)–2(F1) originate from relatively small droplets with $R_D \approx 100$ nm. The average radial distances d of the clusters from the droplet centers and their root mean square deviations extracted from Figs. 2(B2)–2(D2) are compiled in Table I, and a more detailed account of the cluster positions and sizes is given in Table S2 in the SM [15]. The Xe clusters in Figs. 2(B2)–2(D2) appear as nearly round, tightly localized density peaks, while those in Figs. 2(E2) and 2(F2) are significantly elongated along a common axis within each droplet. Similarly to previous imaging studies of rotating nanodroplets [6,10], we interpret these patterns as 2D projections of Xe clusters that are attached to vortices inside He nanodroplets with different

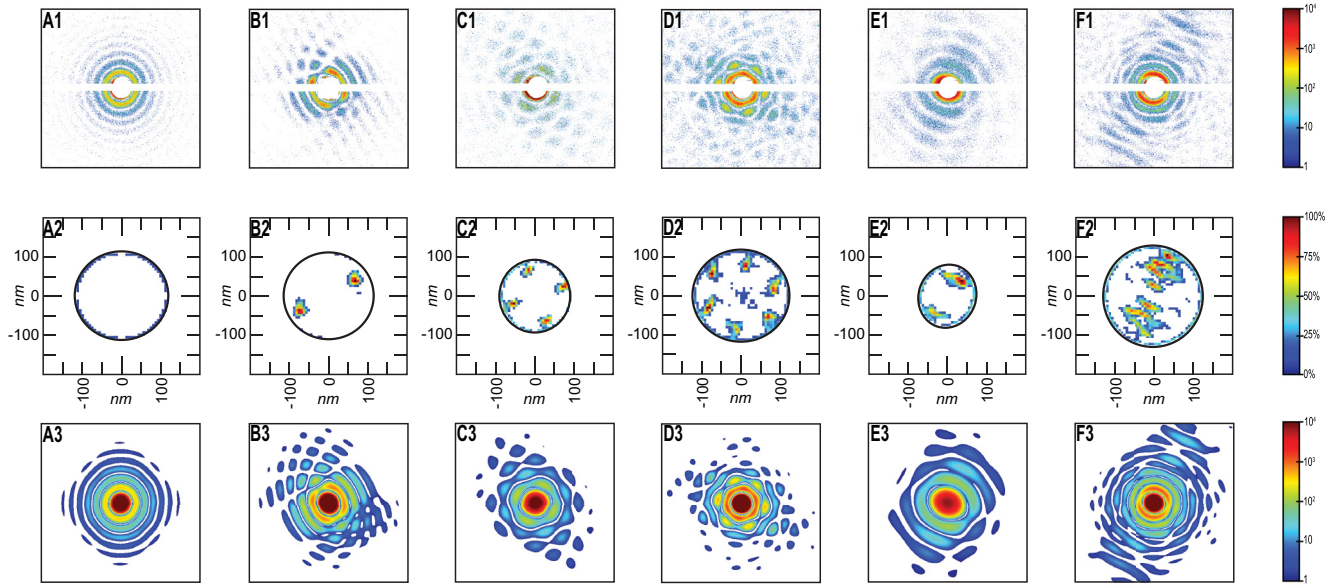

FIG. 2. Diffraction patterns of pure (A1) and Xe-doped (B1)–(F1) helium droplets. Each image is generated by illuminating a single droplet with a single XFEL pulse. All diffraction images are displayed in a logarithmic color scale as indicated on the right. The Xe densities shown in (B2)–(F2) in linear scale were derived using the DCDI iterative phase retrieval algorithm. (A3)–(F3) show calculated diffraction patterns arising from the He droplets and dopant Xe clusters depicted in (A2)–(F2). In particular, the configurations (A2)–(D2) were also reproduced by an analytical treatment as described in the SM [15]. Both the experimental data and the calculated diffraction patterns have been cropped to show the central 450 × 450 pixel portions of the complete 1024 × 1024 images.

axes of rotation. In particular, Figs. 2(B2)–2(D2) correspond to droplets that rotate along an axis perpendicular to the image plane, i.e., pointing toward the observer, while the axes of rotation for droplets (E2) and (F2) are significantly tilted with respect to the direction of observation. The fact that the cluster filament projections in Figs. 2(B2)–2(D2) have circular shapes indicates that the images were recorded approximately along the filament axis. From the size of the density spots, and assuming filament lengths on the order of $\approx R_D$ as in Figs. 2(E2) and 2(F2), the relative angle between the filament axis and the line of sight is estimated to be within $0 \pm 15^\circ$ for Figs. 2(B2)–2(D2). Therefore, the measured radial distance of the center of gravity of the intensity spots in Table I approximately gives the distance of the vortices from the rotational axis. The high symmetries of the density distributions, in particular, in Figs. 2(C2) and 2(D2) serve as an additional indication for on-axis imaging. The following discussion will focus on symmetric patterns of two, four, and six vortices. This selection is by no means representative of the entire range of possible vortex configurations in the nanodroplets. It rather reflects the limited amount of images we were able to obtain within the available beamtime. All droplets in Figs. 2(A2)–2(F2) exhibit several common attributes that will be discussed in the following.

TABLE I. Measured parameters for droplets shown in Figs. 2(B2)–2(D2). The errors reflect the root mean square deviation of the parameters.

Number of clusters	2	4	6
R_D (nm)	108 ± 6	90 ± 5	118 ± 6
d (nm)	83 ± 8	71 ± 5	92 ± 5
d/R_D	0.77	0.79	0.78
N_{He}	1.2×10^8	6.9×10^7	1.5×10^8
N_{Xe} (total)	2.9×10^5	3.7×10^5	6.0×10^5

All clusters in Figs. 2(B2)–2(D2) reside at symmetrically arranged positions far away from each other and at large radii relative to the droplet center. In the absence of vortices, the van der Waals interaction between an embedded particle and an isotropic, spherical droplet leads to a potential energy minimum at the droplet's center [22], which is expected to confine the dopant clusters to $d < 0.3 \cdot R_D$ for He droplets and Xe clusters with sizes similar to those in Table I. However, the Xe clusters are located more than twice as far away from the droplet center as predicted by the isotropic droplet model. Moreover, in an isotropic droplet such clusters would recombine before the droplet would reach the imaging x-ray beam [23]. The widely spaced Xe cluster positions, therefore, support the above interpretation that they represent the locations of vortices that trap the Xe aggregates far from the center, with the repulsion between vortices preventing their recombination into a single large cluster.

Since Xe atoms collide with the droplet randomly during its traversal of the pickup cell, the atoms will move randomly inside the droplet following capture, sampling different volume elements of the droplet with the same probability. After thermalization, the velocity distribution of the Xe atoms will be biased by the rotation of the droplet. The upper boundary of this velocity is given by the equatorial velocity of the rotating droplet of ≈ 1 m/s, given by the angular velocity of $10^7\ \mathrm{s}^{-1}$ and the droplet radius $R = 100$ nm. This maximum rotational velocity is much smaller than the thermal velocity of Xe atoms of about 10 m/s at a droplet temperature of $T \approx 0.8$ K in the pickup cell [12]. Therefore, the distribution of the thermalized Xe atoms is dominated by thermal motion,

which also spans every volume element of the droplet evenly. Moreover, the markedly similar partitioning of Xe atoms between different large clusters (see Table S2 [15]) within each droplet in Figs. 2(B2), 2(C2), and 2(D2) indicates that they must be assembled from large numbers of atoms or subclusters. Therefore, all vortices in the droplets are expected to be traced by Xe atoms and the probability to have an empty vortex is negligible due to Poisson statistics.

Packard and co-workers also imaged configurations of two, four, and six vortices in bulk superfluid He within a 2 mm wide rotating cylinder [24,25]. They concluded that the vortices in those experiments adopted symmetric arrangements similar to the presently observed configurations, but at smaller separations relative to the size of the container. For two vortices in a cylinder, the ratio of vortex separation to cylinder diameter is $x_0 \approx 0.125$, compared with the ratio of $d/R_D = 0.77$ for two vortices in a droplet. Similarly, four and six vortices are observed at $d/R_D = 0.79$ and 0.78, respectively. According to Hess [26], two vortices are stable when $x_0 < 0.25$. The free energy of two vortices exceeds that of a single vortex in a rotating cylinder when $x_0 >\sim 0.25$, although an activation barrier exists for a transition from two vortices to one. Two vortices remain metastable until the barrier disappears at $x_0 > 0.55$, and only a single vortex solution is possible. Thus, multiple vortices are thermodynamically preferred very close to the center, and are never expected beyond $x_0 > 0.55$. Very recently, the positions of vortices in droplets with $\sim$5 nm radii were calculated via density functional theory [27]. These calculations also predict much smaller radial displacements of the vortices inside rotating droplets than described herein, similar to previous measurements [24,25] and calculations for a rotating cylinder [26,28]. Additionally, these works all report the presence of a central vortex in systems containing six or seven vortices, which is absent in our measurements. While the reconstruction shows diffuse density in the central region of Fig. 2(D2), it accounts for less than 2% of the total density and we believe it to be an artifact of the reconstruction, as discussed in more detail in the SM [15].

We propose that the differences between our measurements and previous results stem from the presence of Xe clusters, which contribute to the rotational energy and angular momentum in doped droplets and stabilize vortex configurations with large distances between the vortices and the droplet center. The discrepancies between the measurements and the DFT calculations [27] likely stem from the fact that the calculations were performed for a constant angular velocity compared to the constant angular momentum condition as in the experiment. In addition, doped vortices are repelled from the droplet surface due to the solvation potential of the embedded Xe atoms, which may prevent their annihilation at the surface as in the case of bare vortices. Therefore, configurations of experimentally observable doped droplet vortices may deviate considerably from the bare vortices described by theory [27]. Multiple vortices in a spherical vessel have also been modeled in Ref. [29] by lines that are parallel to the rotation axis and confined to some predetermined configurations such as a ring with and without a central vortex. However, this modeling predicted a central vortex when the number of vortices exceeds two, which is at odds with recent DFT calculations [27]. Therefore, the theoretical modeling of multivortex systems in a droplet seems currently inconclusive. For the purpose of illustration, the effect of Xe on the equilibrium position of a vortex in a cylinder is discussed in SM [15].

The coordinates of the vortices can be used to estimate the angular velocity ω, angular momentum L_V, and rotational energy E_V of the droplet. The shapes and dynamics of bare vortices with fixed boundary conditions can, in principle, be calculated using the Biot-Savart law [30–33]. However, the implementation of this approach is not straightforward due to the additional acquired mass of the dopant atoms and a possible vorticity dependence of the droplet shape. For the purpose of an estimate we assumed that a doped vortex has the same shape and angular velocity as the bare vortex with 10 nm core diameter in a spherical He droplet. The diameter was estimated for uniform Xe filaments of length R_D with the density of solid Xe. The values of L_V, E_V, and ω were calculated numerically [34,35] for a single vortex with the closest approach to the rotational axis set equal to the measured values of d. When multiple vortices are present at large d, the motion of the vortices is predominantly governed by their self-induced velocity, whereas contributions from the velocity fields of other vortices are small. Thus, their angular momenta and energies are approximately additive. The values of L and E for the Xe content of the vortex are calculated using the angular velocity ω of the vortices and the mass of the Xe clusters at distance d from the droplet center. For example, the two vortices in Fig. 2(B2) have a total angular momentum $L_V = 1.8 \times 10^7\,\hbar$ and a rotational energy $E_V = 1.1 \times 10^3$ K with $\omega = 7.3 \times 10^6$ rad/s. Attached Xe clusters containing a total $N_{\mathrm{Xe}} = 2.9 \times 10^5$ atoms carry an additional $L_{\mathrm{Xe}} = 3.1 \times 10^7\,\hbar$ and $E_{\mathrm{Xe}} =$ 860 K. For comparison the angular momentum and kinetic energy of a bare single central straight vortex with a core diameter of 10 nm in the $R_D = 108$ nm droplet are $1.2 \times 10^8\,\hbar$ and 5.0×10^3 K, respectively [34,35]. We note that the limited information on the 3D shape of the embedded Xe clusters leads to a corresponding relatively large uncertainty in the exact partitioning of angular momentum and rotational energy between the host droplets and the Xe dopants. The qualitative results, however, are unaffected by the exact shapes of the Xe clusters.

It is evident that Xe atoms carry a considerable fraction of the rotational energy and angular momentum of the doped droplets. Doping with Xe atoms causes the evaporation of about half of the He atoms in the droplet under the present experimental conditions, but it remains unclear how much angular momentum is removed via evaporation. As Xe atoms attach to a vortex, they adopt the angular velocity of its revolution about the droplet center. Since the added mass "borrows" angular momentum from the vortex, the vortex must compensate by moving outward, resulting in the larger equilibrium distances of the vortices observed in this work. The fact that similar numbers of atoms were found in symmetric vortices (see Table S2 [15]) is consistent with the conservation of the number of vortices upon doping. We note that the initial configurations of bare vortices before doping can deviate considerably from the experimentally determined configurations of doped vortices, but they cannot be accessed in this work. Ultimately, doped vortices cannot approach the surface beyond a certain extent due to the decrease of solvation energy of Xe clusters close to the surface [22]. Hence, upon reaching some critical proximity to the surface (that is

currently unknown) the vortices must become unstable and vanish. Then, Xe clusters orbiting on the periphery of the superfluid droplet will carry the entire angular momentum and rotational energy. In the absence of vortices, the van der Waals attraction between Xe clusters will likely lead to their agglomeration into a single aggregate and prevent observation of symmetric structures as described herein. Therefore, the findings presented here emphasize that the motion of vortices and dopants pinned to them mutually influence one another and should be considered as a coupled system, the detailed kinematics of which remain largely unknown.

The observation of multiple, widely spaced Xe clusters forming symmetrical configurations in He droplets point to the existence of multiple quantum vortices to which the clusters are attached. The typical distances of the vortices from the droplet center are about 0.7–0.8 of the droplet radius R_D, much larger than expected from previously observed bare vortices in a rotating cylinder of bulk superfluid He (0.1–0.2 R) [24,25] and from recent DFT calculations for small nanodroplets [27]. Bare vortices at such large separations are expected to be unstable, indicating that the presence of Xe clusters stabilizes vortices far from the droplet center. Our work demonstrates that stable vortices exist in He droplets as small as 180 nm in diameter. The existence of vortices in droplets less than 10 nm in diameter has been predicted theoretically [27,36,37]. In this work, however, droplets with radii less than ≈90 nm could not be imaged due to the limited x-ray scattering intensity. With the currently available pulse energies of x-ray free-electron lasers, a focus size of 0.01 μm^2 or less would be required to interrogate droplets as small as 10 nm in diameter and to search for vortices in the smallest droplets predicted to contain them. The presented results call for further theoretical investigations of systems containing a small numbers of vortices to ascertain the wave functions of self-contained, isolated, nanoscale superfluids.

This work was supported by NSF Grant DMR-1501276 (A.F.V.) at USC, by the US Department of Energy, Office of Basic Energy Sciences (DOE, OBES) Chemical Sciences, Geosciences and Biosciences Division, through Contracts No. DE-AC02-05CH11231, No. DE-AC02-06CH11357, and No. DE-AC02-76SF00515 and by the Max Planck Society by funding the development and operation of the CAMP instrument within the ASG at CFEL. Portions of this research were carried out at the Linac Coherent Light Source, a national user facility operated by Stanford University on behalf of the US DOE, OBES under beamtime grant L549: Imaging of quantum vortices in superfluid helium droplets. Sebastian Schorb took part in and provided valuable expertise for the measurements taken during LCLS AMO 54912 beamtime of July 2012 as part of the AMO team. Martin Seifrid and Justin Kwok participated as part of the USC team.

[1] R. P. Feynman, Application of quantum mechanics to liquid helium, in *Progress in Low Temperature Physics*, edited by C. J. Gorter (North-Holland, Amsterdam, 1955), pp.1–53.

[2] R. J. Donnelly, *Quantized Vortices in Helium II*, Cambridge Studies in Low Temperature Physics, edited by A. M. Goldman, P. V. E. McKlintock, and M. Springford (Cambridge University Press, Cambridge, 1991), Vol. 3.

[3] L. Pitaevskii and S. Stringari, *Bose-Einstein Condensation*, The International Series of Monographs on Physics, edited by J. Birman, S. F. Edwards, R. Friend, C. H. LLewellyn-Smith, M. Rees, D. Sherrington, and G. Veneziano (Clarendon, Oxford, 2003), Vol. 116, p. 382.

[4] D. R. Tilley and J. Tilley, *Superfluidity and Superconductivity* (Institute of Physics, Bristol, 1990).

[5] S. Grebenev, J. P. Toennies, and A. F. Vilesov, Superfluidity within a small helium-4 cluster: The microscopic Andronikashvili experiment, Science **279**, 2083 (1998).

[6] L. F. Gomez, E. Loginov, and A. F. Vilesov, Traces of Vortices in Superfluid Helium Droplets, Phys. Rev. Lett. **108**, 155302 (2012).

[7] M. Hartmann, R. E. Miller, J. P. Toennies, and A. Vilesov, Rotationally Resolved Spectroscopy of SF_6 in Liquid-Helium Clusters—A Molecular Probe of Cluster Temperature, Phys. Rev. Lett. **75**, 1566 (1995).

[8] P. Thaler, A. Volk, F. Lackner, J. Steurer, D. Knez, W. Grogger, F. Hofer, and W. E. Ernst, Formation of bimetallic core-shell nanowires along vortices in superfluid He nanodroplets, Phys. Rev. B **90**, 155442 (2014).

[9] D. Spence, E. Latimer, C. Feng, A. Boatwright, A. M. Ellis, and S. F. Yang, Vortex-induced aggregation in superfluid helium droplets, Phys. Chem. Chem. Phys. **16**, 6903 (2014).

[10] L. F. Gomez, K. R. Ferguson, J. P. Cryan, C. Bacellar, R. M. P. Tanyag, C. Jones, S. Schorb, D. Anielski, A. Belkacem, C. Bernando, R. Boll, J. Bozek, S. Carron, G. Chen, T. Delmas, L. Englert, S. W. Epp, B. Erk, L. Foucar, R. Hartmann, A. Hexemer, M. Huth, J. Kwok, S. R. Leone, J. H. S. Ma, F. R. N. C. Maia, E. Malmerberg, S. Marchesini, D. M. Neumark, B. Poon, J. Prell, D. Rolles, B. Rudek, A. Rudenko, M. Seifrid, K. R. Siefermann, F. P. Sturm, M. Swiggers, J. Ullrich, F. Weise, P. Zwart, C. Bostedt, O. Gessner, and A. F. Vilesov, Shapes and vorticities of superfluid helium nanodroplets, Science **345**, 906 (2014).

[11] R. M. Tanyag, C. Bernando, C. F. Jones, C. Bacellar, K. Ferguson, D. Anielski, R. Boll, S. Carron, J. Cryan, L. Englert, S. Epp, B. Erk, L. Foucar, L. Gomes, R. Hartmann, D. Neumark, D. Rolles, B. Rudek, K. Siefermann, J. Ullrich, F. Weise, C. Bostedt, O. Gessner, and A.F. Vilesov, X-ray coherent diffraction imaging by immersion in nanodroplets, Struct. Dyn. **2**, 051102 (2015).

[12] L. F. Gomez, E. Loginov, R. Sliter, and A. F. Vilesov, Sizes of large helium droplets, J. Chem. Phys. **135**, 154201 (2011).

[13] J. P. Toennies and A. F. Vilesov, Superfluid helium droplets: A uniquely cold nanomatrix for molecules and molecular complexes, Angew. Chem. Int. Ed. **43**, 2622 (2004).

[14] F. Stienkemeier and K. K. Lehmann, Spectroscopy and dynamics in helium nanodroplets, J. Phys. B **39**, R127 (2006).

[15] See Supplemental Material at http://link.aps.org/supplemental/10.1103/PhysRevB.93.180510 for the results of algebraic modeling of symmetric diffraction patterns. It also describes the determination of the number of embedded Xe atoms. In addition, it contains an illustration of the effect of Xe on the equilibrium position of a vortex in a cylinder.

[16] G. P. Bewley, D. P. Lathrop, and K. R. Sreenivasan, Superfluid helium—Visualization of quantized vortices, Nature (London) **441**, 588 (2006).

[17] C. Bostedt, J. D. Bozek, P. H. Bucksbaum, R. N. Coffee, J. B. Hastings, Z. Huang, R. Lee, W. S. Schorb, J. N. Corlett, P. Denes, P. Emma, R. W. Falcone, R. W. Schoenlein, G. Doumy, E. P. Kanter, B. Kraessig, S. Southworth, L. Young, L. Fang, M. Hoener, N. Berrah, C. Roedig, and L. F. DiMauro, Ultra-fast and ultra-intense x-ray sciences: first results from the Linac Coherent Light Source free-electron laser, J. Phys. B **46**, 164003 (2013).

[18] K. R. Ferguson, M. Bucher, J. D. Bozek, S. Carron, J.-C. Castagna, R. Coffee, G. I. Curiel, M. Holmes, J. Krzywinski, M. Messerschmidt, M. Minitti, A. Mitra, S. Moeller, P. Noonan, T. Osipov, S. Schorb, M. Swiggers, A. Wallace, J. Yina, and C. Bostedt, The atomic, molecular and optical science instrument at the Linac coherent light source, J. Synchr. Rad. **22**, 492 (2015).

[19] L. Strüder, S. Epp, D. Rolles, R. Hartmann, P. Holl, G. Lutz, H. Soltau, R. Eckart, C. Reich, K. Heinzinger, C. Thamm, A. Rudenko, F. Krasniqi, K. U. Kuhnel, C. Bauer, C. D. Schroter, R. Moshammer, S. Techert, D. Miessner, M. Porro, O. Halker, N. Meidinger, N. Kimmel, R. Andritschke, F. Schopper, G. Weidenspointner, A. Ziegler, D. Pietschner, S. Herrmann, U. Pietsch, A. Walenta, W. Leitenberger, C. Bostedt, T. Moller, D. Rupp, M. Adolph, H. Graafsma, H. Hirsemann, K. Gartner, R. Richter, L. Foucar, R. L. Shoeman, I. Schlichting, and J. Ullrich, Large-format, high-speed, X-ray pnCCDs combined with electron and ion imaging spectrometers in a multipurpose chamber for experiments at 4th generation light sources, Nucl. Instrum. Meth. A **614**, 483 (2010).

[20] D. Rupp, M. Adolph, T. Gorkhover, S. Schorb, D. Wolter, R. Hartmann, N. Kimmel, C. Reich, T. Feigl, A. R. B. de Castro, R. Treusch, L. Struder, T. Moller, and C. Bostedt, Identification of twinned gas phase clusters by single-shot scattering with intense soft x-ray pulses, New J. Phys. **14**, 055016 (2012).

[21] J. R. Fienup, Reconstruction of an object from modulus of its Fourier-transform, Opt. Lett. **3**, 27 (1978).

[22] K. K. Lehmann, Potential of a neutral impurity in a large He-4 cluster, Mol. Phys. **97**, 645 (1999).

[23] E. Loginov, L. F. Gomez, N. Chiang, A. Halder, N. Guggemos, V. V. Kresin, and A. F. Vilesov, Photoabsorption of Ag_N ($N \sim$ 6–6000) Nanoclusters Formed in Helium Droplets: A Transition from Compact to Multi-Center Aggregation, Phys. Rev. Lett. **106**, 233401 (2011).

[24] E. J. Yarmchuk, M. J. V. Gordon, and R. E. Packard, Observation of Stationary Vortex Arrays in Rotating Superfluid-Helium, Phys. Rev. Lett. **43**, 214 (1979).

[25] E. J. Yarmchuk and R. E. Packard, Photographic studies of quantized vortex lines, J. Low Temp. Phys. **46**, 479 (1982).

[26] G. B. Hess, Angular momentum of superfluid helium in a rotating cylinder, Phys. Rev. **161**, 189 (1967).

[27] F. Ancilotto, M. Pi, and M. Barranco, Vortex arrays in nanoscopic superfluid helium droplets, Phys. Rev. B **91**, 100503(R) (2015).

[28] F. Ancilotto, M. Pi, and M. Barranco, Vortex arrays in a rotating superfluid He-4 nanocylinder, Phys. Rev. B **90**, 174512 (2014).

[29] S. T. Nam, G. H. Bauer, and R. J. Donnelly, Vortex patterns in a freely rotating superfluid, J. Korean Phys. Soc. **29**, 755 (1996).

[30] K. W. Schwarz, Three-Dimensional vortex dynamics in superfluid He-4: Line-line and line-boundary interactions, Phys. Rev. B **31**, 5782 (1985).

[31] R. Hanninen and A. W. Baggaley, Vortex filament method as a tool for computational visualization of quantum turbulence, Proc. Natl. Acad. Sci. USA **111**, 4667 (2014).

[32] H. Adachi, S. Fujiyama, and M. Tsubota, Steady-state counterflow quantum turbulence: Simulation of vortex filaments using the full Biot-Savart law, Phys. Rev. B **81**, 104511 (2010).

[33] S. Yui and M. Tsubota, Counterflow quantum turbulence of He-II in a square channel: Numerical analysis with nonuniform flows of the normal fluid, Phys. Rev. B **91**, 184504 (2015).

[34] G. H. Bauer, R. J. Donnelly, and W. F. Vinen, Vortex configurations in a freely rotating superfluid drop, J. Low Temp. Phys. **98**, 47 (1995).

[35] K. K. Lehmann and R. Schmied, Energetics and possible formation and decay mechanisms of vortices in helium nanodroplets, Phys. Rev. B **68**, 224520 (2003).

[36] F. Dalfovo, R. Mayol, M. Pi, and M. Barranco, Pinning of Quantized Vortices in Helium Drops by Dopant Atoms and Molecules, Phys. Rev. Lett. **85**, 1028 (2000).

[37] M. Barranco, R. Guardiola, S. Hernandez, R. Mayol, J. Navarro, and M. Pi, Helium nanodroplets: An overview, J. Low Temp. Phys. **142**, 1 (2006).